Atmos. Chem. Phys. Discuss., 10, 7469–7494, 2010
www.atmos-chem-phys-discuss.net/10/7469/2010/

Atmospheric Chemistry and Physics Discussions

This discussion paper is/has been under review for the journal Atmospheric Chemistry and Physics (ACP). Please refer to the corresponding final paper in ACP if available.

Optical closure experiments for biomass smoke aerosols

L. E. Mack[1], E. J. T. Levin[1], S. M. Kreidenweis[1], D. Obrist[2], H. Moosmüller[2], K. A. Lewis[3], W. P. Arnott[3], G. R. McMeeking[1,*], A. P. Sullivan[1], C. E. Wold[4], W.-M. Hao[4], J. L. Collett Jr.[1], and W. C. Malm[5]

[1]Department of Atmospheric Science, Colorado State University, Fort Collins, CO, USA
[2]Desert Research Institute, Nevada System of Higher Education, Reno, NV, USA
[3]Department of Physics, University of Nevada, Reno, NV, USA
[4]US Forest Service, RMRS Fire Sciences Laboratory, Missoula, MT, USA
[5]Air Resources Division, US National Park Service, Fort Collins, CO, USA
[*]now at: Centre for Atmospheric Science, University of Manchester, Manchester, UK

Received: 1 March 2010 – Accepted: 12 March 2010 – Published: 23 March 2010

Correspondence to: S. M. Kreidenweis (sonia@atmos.colostate.edu)

Published by Copernicus Publications on behalf of the European Geosciences Union.

Abstract

The FLAME experiments were a series of laboratory studies of the chemical, physical, and optical properties of fresh smokes from the combustion of wildland fuels that are burned annually in the western and southeastern US. The burns were conducted in the combustion chamber of the USFS Fire Sciences Laboratory in Missoula, Montana. Here we discuss the retrieval of optical properties for a variety of fuels burned in FLAME 2, using nephelometer-measured scattering coefficients, photoacoustically-measured aerosol absorption coefficients, and size distribution measurements. Uncertainties are estimated from the various instrument characteristics and from instrument calibration studies. Our estimates of single scattering albedo for different dry smokes varied from 0.43–0.99, indicative of the wide variations in smoke aerosol chemical composition that were observed. In selected case studies, we retrieved the complex refractive index from the measurements, but show that these are highly sensitive to the uncertainties in measured size distributions.

1 Introduction

Absorbing aerosols represent large contributions to the aerosol optical depth (AOD) attributed to "atmospheric brown clouds" (Ramanathan et al., 2007), which have been shown to have widespread effects on climate due to the surface dimming and atmospheric solar heating with which they are associated. Ramanathan and Feng (2009) discuss a variety of impacts attributable to atmospheric brown clouds: for example, the absorption of light and the resulting heating affects atmospheric dynamics locally by stabilizing atmospheric temperature profiles and on larger scales by affecting monsoon circulations, and deposition of absorbing aerosols onto snow and ice can accelerate melting. As discussed by Bond (2007), the annual mass emissions of carbonaceous aerosol species (organic carbon, OC, and elemental carbon, EC) from open biomass burning are very large compared with the total emissions from energy-related combus-

ACPD

10, 7469–7494, 2010

tion, and thus should be considered in strategies aimed at reducing radiative forcing by warming aerosols. The optical properties of biomass burning aerosols at visible wavelengths are of interest since a large fraction of incoming solar energy is in this range (Chen and Bond, 2010), and since carbonaceous aerosols contribute to visibility degradation, sometimes in complex ways (Moosmüller et al., 2009).

Calculated climate and visibility impacts of biomass burning aerosols are sensitive to the relative amounts of scattering and absorption, which in turn depend on the size distribution of the particles and on composition (Chylek and Wong, 1995). Chen and Bond (2010) note the high variability observed in the optical properties of particles emitted from biomass combustion, reflecting not only variations in fuel type but also in fuel size and combustion conditions. Further, optical properties are affected by the often complex shapes of combustion particles (Moosmüller et al., 2009) and by water uptake at elevated relative humidities (Massoli et al., 2009).

In this study, we focus on contributing to the database of knowledge of the optical properties of biomass burning particles that have not been processed in the atmosphere, via laboratory measurements made on dry particles within a few hours of emission from open burning. We further relate these optical properties to measured bulk particle composition to show the extent to which simple assumptions can be used to model scattering and absorption coefficients.

2 Experimental

The Fire Laboratory at Missoula Experiments (FLAME) were performed at the U.S. Forest Service Fire Science Lab (FSL) in Missoula, Montana, and were designed specifically to address data gaps in the characterization of gas- and particulate-phase emissions from fuels commonly burned in the United States during wildfires and prescribed burns. The wide variety of fuels burned also provided an opportunity to investigate the range of optical properties of the aerosols produced by biomass burning, and to seek relationships between the physical and optical properties of the aerosols. McMeeking

ACPD
10, 7469–7494, 2010

et al. (2009) provide a complete description of the fuels, burn conditions, instrumentation, and analytical methods, and gas- and particulate-phase emission factors for both the FLAME 1 (2006) and FLAME 2 (2007) studies. In this work, we report data from the FLAME 2 study, which was conducted 20 May–6 June 2007, and specifically from the chamber burn portion of the study which was designed to obtain data for an optical closure study.

During FLAME 2, a total of 21 chamber burns were performed using 18 fuels; two fuels were burned twice and several fuels were burned in mixtures (Table 1). Approximately 200 g of each fuel or fuel mixture was ignited and allowed to burn completely, with the emissions filling the sealed combustion chamber (12.5×12.5×19.5 m). As shown by McMeeking et al. (2009), the emissions were well-mixed through the volume within about 30 min after ignition. Emissions were continuously sampled from the combustion chamber into a ≈200 l drum at a flow rate of ≈1000 lpm, and ≈200 lpm were sampled from the drum into an adjacent laboratory which housed our instrumentation. A sampling manifold pulled ≈30 lpm from this stream, and supplied continuous samples to each instrument used in this work. The total residence time of the sample between the chamber and our instruments was approximately 25 s. Emissions were typically sampled for two hours before the chamber was diluted with clean outside air and prepared for the next experiment. The aerosol samples had values of RH<35% at the points of measurement.

Simultaneous measurements were made of scattering and absorption coefficients, aerosol size distribution, and aerosol composition. Measurements of the absorption coefficient, b_{abs}, were made every 2 min using a photoacoustic spectrometer (PAS) operating at 532 nm (Arnott et al., 1999, 2000; Lewis et al., 2008). The PAS was calibrated as described by Arnott et al. (2000) prior to the FLAME 2 study using ammonium sulfate and kerosene smoke aerosol particles. Scattering coefficient, b_{scat}, measurements were made using a three wavelength nephelometer (TSI 3563) operating at 450, 550 and 700 nm. The nephelometer was calibrated using filtered air, CO_2, and SUVA (HFC, 134a) gas prior to the study (Anderson and Ogren, 1998) and the calibrations

ACPD
10, 7469–7494, 2010

were checked again at the conclusion of the study. Values of b_{scat} were measured every two seconds and were interpolated to 532 nm using the observed Ångström scattering exponent between 450 and 550 nm. Corrections to measured b_{scat} were also made for angular non-idealities following Anderson and Ogren (1998), assuming only submicron particles were present. Measurements of b_{scat} and b_{abs} were averaged over 10-min intervals to match the sampling times of the size distributions.

Aerosol size distributions were measured using the CSU aerosol sizing rack (Hand and Kreidenweis, 2002), which included a differential mobility particle sizer (DMPS; TSI 3081 differential mobility analyzer with TSI 3785 water-based condensation particle counter) and an optical particle counter (OPC; PMS Lasair 1003). The DMPS scans were conducted over 10 min intervals and a mobility diameter range from 0.04–0.63 µm. OPC data were acquired in 6 channels, from nominal sizes of 0.2 to 2.0 µm, over the same time interval. As discussed in detail in Levin et al. (2010), size distributions were constructed for the diameter range of 0.04–2.0 µm from the combined DMPS+OPC data set using the alignment method of Hand and Kreidenweis (2002). Since highly absorbing aerosols cause the OPC to underestimate particle size, leading to biased size distributions, some of the resulting aligned distributions did not pass quality control checks, and the DMPS-only size distributions were instead used in this work, as explained further below.

Samples of particulate matter with aerodynamic diameters of less than 2.5 ($PM_{2.5}$) and 10 µm (PM_{10}) were collected onto Teflon, nylon, and quartz filters during each burn using the IMPROVE sampler and analyzed for the mass concentrations of inorganic ions, organic carbon (OC), elemental carbon (EC), and elements. The carbon analyses for these samples followed the thermal-optical reflectance (TOR) protocal used in the IMPROVE network (Chow et al., 1993, 2004, 2007). The Teflon filters were weighed before and after each experiment to determine total gravimetric mass under approximately dry conditions (relative humidity, RH≤40%). Additionally a high volume sampler (Hi-Vol) with a $PM_{2.5}$ size cut collected samples on quartz fiber filters. Filter punches from the Hi-Vol samples were analyzed by a Sunset Labs carbon analyzer

using the thermal-optical tranmission (NIOSH) protocol (Bae et al., 2004) to obtain measurements of organic and elemental carbon mass concentrations, as described in Sullivan et al. (2008). Although total carbon aerosol concentrations from the two methods agreed well, they differed significantly in the fractions assigned to EC and OC (McMeeking et al., 2009). Complete descriptions of the aerosol size distribution measurements and of the derivation of aerosol composition using the filter-based data are provided in Levin et al. (2010).

Scattering coefficient, absorption coefficient, and size distribution data were not used during periods where concentrations were rapidly changing, such as at the start of the burn. Further, some of the instrument responses were saturated at the beginning of burns when aerosol concentrations were high, and therefore these data points were also removed from our analyses. Since on average each burn sampling period lasted 2 h (the combustion of the fuel typically was completed within 5–15 min), the 10-min resolution of our data led to a maximum number (N) of ≈12 data points for each experiment.

3 Results and discussion

3.1 Measured single scattering albedos

Single scattering albedo, ω, is the ratio of the aerosol scattering coefficient, b_{scat}, to the total extinction coefficient, b_{ext}, where b_{ext} is the sum of scattering and absorption coefficients, $b_{\mathrm{scat}}+b_{\mathrm{abs}}$. In this study, we estimated ω in two ways; first, by directly calculating it from measured scattering and absorption coefficients (ω_{meas}), and second, by computing it using measured size distributions and estimated refractive indices (ω_{calc}), as explained in Sect. 3.2 below.

Although particle number and mass concentrations and the measured values of b_{scat} and b_{abs} decreased over the course of an experiment, the calculated values of ω_{meas} were relatively constant with time, with a mean standard deviation of ±0.007. We

thus report a value of ω_{meas} for each experiment that has been averaged over all valid sampling times. The relative uncertainty in ω_{meas} was calculated as

$$\frac{\Delta\omega_{meas}}{\omega_{meas}} = \sqrt{\left(\frac{b_{scat}}{b_{scat}+b_{abs}}\Delta b_{bs}\right)^2 + \left(\frac{b_{abs}}{b_{scat}+b_{abs}}\Delta b_{scat}\right)^2} \quad (1)$$

where Δb_{scat} was assumed to be ±10% (Anderson et al. 1996) and Δb_{abs}±5% (Lewis et al., 2008). The calculated values of ω_{meas} for the chamber burns are listed in Table 1. Values ranged from 0.43 to 0.99. Fuel species/samples burned in multiple experiments demonstrated consistency between replicate measurements of ω. Smoke from two separate burns of Alaskan duff had ω_{meas} of 0.97 and 0.99, and the aerosols from two black needlerush burns had ω_{meas} of 0.92 and 0.90. Longleaf pine needles and wiregrass were each burned separately producing smoke with ω_{meas} values of 0.95 and 0.85, respectively, while a mixture of the two fuels produced aerosols with a ω_{meas} of 0.93, between that of the individual fuels. Douglas fir needles and branches were burned three times: twice using dry fuel and producing ω_{meas} values of 0.96 and 0.98, and once using fresh fir needles and branches, which produced smoke with ω_{meas} of 0.53. The relatively large difference in values of ω_{meas} obtained for dry and fresh Douglas fir samples indicate that the condition of the fuel and subsequent combustion conditions play a large role in the optical properties of emitted aerosols. It is also interesting to note the differences in ω_{meas} for samples of palmetto leaves obtained from Florida (ω_{meas}=0.43) and from Mississippi (ω_{meas}=0.62). As shown in Levin et al. (2010), the chemical compositions of these two smokes were somewhat different, reflecting differences in fuel composition and fuel moisture content or in combustion conditions, that are then also manifested in differing ω_{meas}.

It is well known that particulate emissions vary considerably between the flaming and smoldering phases of combustion, and Reid et al. (2005) suggested relationships between the combustion conditions and the ω of the smoke aerosol. In McMeeking et al. (2009), we used the fire-integrated modified combustion efficiency (MCE; Ward and Radke, 1993) as an indicator of the combustion conditions dominating the burn, where

ACPD
10, 7469–7494, 2010

MCE is the ratio of the molar concentration of CO_2 to the summed molar concentrations of CO_2+CO in the emissions. MCE values lower than ~0.8 indicate predominantly smoldering phase conditions; MCE values higher than ~0.9 indicate flaming phase dominated combustion. We found no correlation (r^2=0.006) between ω_{meas} and fire-integrated MCE values for the FLAME 2 chamber burns, consistent with our observations that the relationship between MCE and the ratio of EC to total aerosol carbon was not strong (McMeeking et al., 2009). Further, each of the chamber experiments included a mix of smoke from flaming and smoldering phases, preventing a clear examination of the relationship between combustion phase and optical properties. Reid et al. (2005) also showed that ω_{meas} was dependent on the type and origin of the fuel. For the limited number of samples we obtained, the combustion of southeastern and desert shrubs yielded aerosols with lower ω_{meas} than the other fuels; duff, fir and pine samples yielded aerosols with the highest ω_{meas}. We explore the links with smoke aerosol chemical composition in Sect. 3.3.

3.2 Retrieval of refractive indices

As demonstrated by Riziq et al. (2007), it is possible to deduce the complex index of refraction of an aerosol sample if simultaneous measurements of size distributions, scattering coefficients, and extinction or absorption coefficients are available. The method relies on the applicability of Mie theory, including the assumption of spherical particles, and the chemical homogeneity of the sample. Our simultaneous measurements of aerosol size distributions, b_{scat}, and b_{abs} were used in a method similar to that of Riziq et al. (2007) to retrieve best-fit complex refractive indices for our experiments. Values of b_{scat} and b_{abs} were calculated, using a Mie routine and the measured size distributions, for an array of assumed complex refractive indices, $m = n + ik$. The components of the complex refractive index were varied between $1.0 < n < 2.5$ and $0 < k < 0.7$ for 400 values each of n and k. The best-fit index of refraction was determined by finding the global minimum of the merit function χ^2/N within the n, k parameter space defined above (Riziq et al., 2007; Dinar et al., 2008), where N is the number of measurements

ACPD
10, 7469–7494, 2010

and χ^2 is the chi-square function:

$$\chi^2 = \sum_{j=1}^{2} \sum_{i=1}^{N} \frac{(y_{\text{meas}} - y_{\text{calc}})_{i,j}^2}{\varepsilon_{i,j_{\text{meas}}}^2 + \varepsilon_{i,j_{\text{calc}}}^2} \quad (2)$$

For this study y_{meas} was the measured value of interest (i.e., b_{scat} or b_{abs}), y_{calc} the corresponding calculated value, $\varepsilon_{\text{meas}}$ the uncertainty associated with the measured quantity, and $\varepsilon_{\text{calc}}$ the uncertainty associated with the calculated quantity. Uncertainties in the retrieved values of n and k were determined as the values which fell within 1σ of the minimum χ^2, as described by Dinar et al. (2008).

At the start of the study, we conducted a calibration test using ammonium sulfate $(NH_4)_2SO_4$ aerosol, a salt which when aerosolized from aqueous solution and dried produces purely scattering, nearly-spherical particles of known density and refractive index. The aerosol was generated into the upstream drum and sampled and characterized in the same way as were the smoke samples. We computed the expected b_{scat} from the measured size distributions, using the literature value of refractive index at mid-visible wavelengths (580 nm), m=1.535+0i (Garland et al., 2007). This calculated b_{scat} was well-correlated with the b_{scat} measured by the nephelometer and corrected for calibration and truncation errors as described in Sect. 2. However, the calculations were lower than the measurements by a factor of 0.884. We attributed this discrepancy to different losses of particles in the sampling systems for the two instruments, and thus adjusted all of the measured size distributions, for both the calibrations and experiments, by dividing by this factor. Using these adjusted aerosol size distributions and the measured values of b_{scat} at 532 nm in Eq. (2), we retrieved a refractive index of 1.538±0.026+0i, in excellent agreement with the expected value. When including the measurements of b_{abs}, which were close to zero, in the retrieval, we obtained 1.541±0.026+0.0003i±0.00003.

We next applied Eq. (2) to retrieve best-fit refractive indices from our measurements of b_{scat} and b_{abs} for smoke aerosols. We selected six cases of varying ω_{meas} for the refractive index retrieval, as shown in Table 3. Table 3 indicates whether DMPS data

ACPD
10, 7469–7494, 2010

alone, or aligned DMPS+OPC data, were used to construct the volume size distribution in each experiment. Sample volume distributions are shown in Fig. 1 (solid black lines). As can be seen from Fig. 1, in some instances the size range of the measurements did not extend to large enough sizes to fully describe the main mode of the $PM_{2.5}$ volume distribution. To help fill this gap, the volume distributions for each valid 10-min sample were fit with monomodal or bimodal lognormal distributions, depending on the best fit to the data (Table 3, and dashed black lines in Fig. 1). The fitted volume distributions were then converted to number distributions assuming particle sphericity, and these number distributions were used in the Mie calculations. Finally, for each burn, a best-fit complex refractive index was retrieved for each individual size distribution measurement (N=1 in Eq. 2), as well as a single-best fit refractive index over all size distributions for that burn (N in Eq. 2 set to the value indicated in Table 3). As a sensitivity test, we applied known counting uncertainties to the size distributions and found that these had no measurable effects on the retrieved refractive indices. Similarly to what was observed for ω_{meas}, individual retrieved values of refractive index did not vary much over an experiment and only the value retrieved by minimizing the error over the entire sample is reported. The retrieved refractive indices corresponding to shape factors=1 (spherical particles assumption) are plotted as the blue symbols in Fig. 2.

It is well-known that combustion particles are often not spherical in shape (Slowik et al., 2004; Chakrabarty et al., 2006). Nonsphericity leads to overestimates of size in the DMPS and has an uncertain effect in the OPC sizing. We tested the sensitivity of the retrieval to the input size distribution by dividing all diameters in the lognormal fit distribution by assumed shape factors of 1.05 to 1.55, in increments of 0.1, and then re-running the retrieval algorithm, resulting in a series of best-fit pairs of n,k for each experiment (Fig. 2). We note that using an assumed shape factor to simply shift the distributions that were obtained by inverting data under the assumption of particle sphericity generates only an approximate estimate of the corrected size distributions (red lines in Fig. 1), since nonsphericity affects the instrument response and should properly be considered in the inversion of the raw data. The strong sensitivity of the

ACPD
10, 7469–7494, 2010

retrieved refractive index to the aerosol size distribution is immediately apparent in Fig. 2. For example, applying a relatively small shape factor of 1.05 produced a 1–5% increase in the retrieved real refractive index, n, and a corresponding 10–18% increase in the imaginary refractive index, k; the differences were larger for larger shape corrections.

There is additional evidence of particle nonsphericity in FLAME smoke particle samples. Hand et al. (2010) used measured volume size distributions and composition-derived densities from the FLAME 1 (2006) chamber burn experiments to estimate aerosol mass concentrations, and compared these to the gravimetric mass determined from filter experiments. In some cases, the computed mass was 60–80% higher than the measured, outside any reasonable uncertainty bounds, indicating that the size distribution measurements were biased (particles sized too large), most likely because of the presence of nonspherical particles. Hand et al. (2010) used these ratios as estimates of the true shape factors and adjusted the size distributions accordingly. In Table 3 we present the ratios of calculated to gravimetric mass concentrations for all six selected experiments, using the size distributions derived assuming a shape factor of 1. We found that this ratio for the chamise experiment was ~1.5 times the measured gravimetric mass concentration, consistent with the factor of 1.6 applied to the FLAME 1 chamise burn studied by Hand et al. (2010). These values of shape factor are in reasonable agreement with prior published estimates. For example, Slowik et al. (2004) and Park et al. (2004) found shape factors of 1.5 and larger for soot particles. In contrast, the mass concentration ratio computed for our black needlerush experiment was 0.79, indicating that the size distributions grossly underestimated the aerosol mass concentrations, most likely because some large particles were not properly sized or were missed entirely when the DMPS data alone were used to construct the $PM_{2.5}$ volume distribution.

3.3 Calculation of refractive indices from composition

Following the approach outlined in Levin et al. (2010), we assumed the measured $PM_{2.5}$ constituents were present as the chemical species with the properties listed in Table 2. Further, we assumed all species were internally mixed and that the particles had zero water content, and used aerosol composition data and a volume-weighted mixing rule to calculate the real (n_{comp}) and imaginary (k_{comp}) indices of refraction. The assumed refractive indices of individual species are shown in Table 2, but special consideration has to be given to the choice of density and complex refractive index for EC which has been shown to be dependent on the void fraction present in the sample (Bond and Bergstrom, 2006). All calculations here were done for the upper and lower limits of the range of refractive index/density pairs reported by Bond and Bergstrom, as indicated in Table 2. Further, we used OC and EC concentrations from both the IMPROVE filters/TOR method ($n_{comp\_IMPROVE}$, $k_{comp\_IMPROVE}$) and from the hi-vol filters/NIOSH protocol (n_{comp_Sunset}, k_{comp_Sunset}). These separate estimates are shown in Fig. 2 as squares and diamonds, with the uncertainty bars indicating the ranges obtained for the two assumed EC properties, as discussed above. The choice of EC properties had a negligible influence on the computed refractive indices for these cases, whereas the differences due to the fraction of total carbonaceous aerosol attributed to EC and OC by the two analysis methods were large for most of the cases.

Comparing the computed and retrieved values in Fig. 2, only in the black needlerush burn was the retrieved real refractive index under the spherical-particles assumption (shape factor=1) smaller than or close to that computed from composition. As shown in Table 3, the black needlerush size distributions very likely underestimated the total aerosol mass concentration. To compensate, the retrieval was forced to a large real refractive index (~1.6, larger than in the other 5 cases), since increases in n increase the computed scattering coefficients. The shape factors estimated from mass concentration ratios for the rice straw, rhododendron, and white spruce experiments (Table 3) were within 10% of unity, which is consistent with the agreement between the opti-

ACPD
10, 7469–7494, 2010

cal properties computed for assumed shape factors between 1.05 and 1.1 and those computed from composition. In contrast, the retrieved real refractive indices for shape factor=1 for the chamise and sagebrush burns, n <1.4, were much lower than expected based on composition. We have already noted that the chamise volume distributions were overestimated because of the presence of nonspherical particles. The mass concentration ratio for sagebrush was very close to 1 (Table 3), suggesting shape factors deviated from unity by less than ∼10%. However, this was contradicted by the measured optical properties: the ω_{meas} of 0.701 was the second lowest of the six cases, indicating a high likelihood that non-spherical particles were present (Chakrabarty et al., 2006). For both the chamise and sagebrush burns, the high absorption led to inaccurate OPC sizing, and DMPS-only distributions were used in our calculations. The computed volume distributions for those burns in particular are thus subject to two strong, but counteracting, biases: they are expected to be overestimated because of the presence of nonspherical particles, and underestimated if significant number concentrations of particles larger than ∼630 nm are present. Depending on the net effects of these influences on the estimated volume distributions, the resulting impacts on the computed optical properties can also be in either direction, towards over- or underestimates of the real refractive index required to match the observed b_{scat}. We note that the composition-derived real refractive indices for sagebrush and chamise are consistent with those retrieved for shape factors of ∼1.23 and 1.55, respectively, and that these shape factors are not unreasonable, based on the available observations. Indeed, for all six cases, the real refractive indices computed from the composition data appear to be good estimates of those required to match the observed b_{scat} for reasonable choices of shape factors (last column, Table 3).

In general, the retrieved values of the imaginary component of the refractive index, k, did not match those computed from chemical composition. Although the choice of carbon analysis method led to little difference between n_{comp_Sunset} and $n_{comp\_IMPROVE}$, there were large differences between k_{comp_Sunset} and $k_{comp\_IMPROVE}$, except for the sagebrush sample. $k_{comp\_IMPROVE}$ was typically larger than k_{comp_Sunset}, reflecting the

ACPD
10, 7469–7494, 2010

larger fraction of total carbon mass assigned to EC by the IMPROVE protocol (Chow et al., 2004). For the choices of shape factors listed in the last column of Table 3, the retrieved k was closer to k_{comp_Sunset} in most of cases.

All of the estimates shown in Fig. 2 assume an internally-mixed aerosol. We checked the effects of this assumption by computing ω from measured aerosol composition using internal- and external-mixture aerosol models. For both models, we adjusted the size distributions by the shape factors shown in the last column of Table 3, which were selected to yield agreement between the retrieved real refractive indices and those calculated from composition. The internal mixture model used these adjusted size distributions and the complex refractive indices derived from composition to calculate the average ω over each experiment. The external-mixture model used a calculated mass extinction efficiency (MEE) and mass absorption efficiency (MAE) for each species individually, applied to measured species mass concentrations, to estimate ω. MEE and MAE were evaluated by computing b_{ext} and b_{abs} for each species using the properties in Table 2 and assuming unit mass distributed as a function of diameter according to the adjusted size distributions.

Figure 3 shows the measured ω together with the results of the internal- and external-mixture model calculations of ω (symbol color) for the IMPROVE and Sunset values of OC and EC (symbol shape) and for the range of complex refractive indices and densities reported by Bond and Bergstrom (2006) for EC (horizontal error bars). As expected, the internal-mixture model always produces an estimate of ω lower than that from the external-mixture model. The variability in the differences between the computed refractive indices applied in the internal-mixture models and the retrieved refractive indices that match ω_{meas} (Fig. 2) is reflected in the variability between the measurements and models in Fig. 3. For example, the internal-mixture model using the EC/OC splits derived from the IMPROVE protocol produced the darkest aerosol and had the poorest agreement with ω_{meas}, except for the chamise sample.

ACPD
10, 7469–7494, 2010

4 Summary and conclusions

Our findings indicated a great deal of variability in ω for biomass burning aerosols, attributable partially to the fuel composition and condition and partially to the combustion conditions. A broad range of ω_{meas} values were observed during this study, with values ranging from 0.43 to 0.99 and with good consistency between replicate burns conducted for a particular fuel. We were not able to find a relationship between fire-integrated MCE and ω_{meas} for our experiments, in part because the experiment was not designed to clearly distinguish between differences in optical properties of emissions from flaming and smoldering combustion phases.

Measured size distributions were the limiting factor in retrieving refractive indices using direct measurements of b_{scat}, b_{abs}, size distributions, and Mie Theory. Measurement of the size distribution was affected by the presence of absorbing particles in the sample, which caused the OPC to underestimate particle size, and by the presence of nonspherical particles, which caused particles to be oversized in the DMPS and had an unknown effect in the OPC. Our calculations demonstrated that small shifts in the measured size distributions, applied to account for particle nonsphericity, had a large impact on the retrieved values of refractive index. Agreement between retrieved real refractive indices and real refractive indices calculated using composition measurements was achieved for reasonable choices of nonsphericity, assuming an internally-mixed aerosol. However, the retrieved imaginary component of refractive index was generally quite different from those computed from composition. Values of $k_{retrieved}$ obtained for the nonsphericity corrections that were applied to force agreement between retrieved and composition-derived real refractive indices generally agreed more closely with those computed for the EC/OC split determined by the NIOSH protocol. As also found in prior studies, the nonsphericity of the particles limited the applicability of both standard aerosol size distribution measurement techniques, and of Mie theory to the computation of optical properties. However, within these constraints, we derived dry refractive indices consistent with ω_{meas} having real components of 1.54–1.67, and

ACPD
10, 7469–7494, 2010

imaginary components of 0.011–0.217.

Measurements of aerosol composition were used to calculate ω using models for externally and internally mixed aerosols. Measured values of ω_{meas} fell between those computed from the two models. Values of ω calculated using an external-mixture model were consistently higher than those using an internal-mixture model, in agreement with previous work that suggested internal mixtures amplify the absorption due to EC (Bond and Bergstrom, 2006).

The observed range in ω_{meas} in this study agrees with the range in the literature (Reid et al., 2005) although we had a larger number of observations with ω_{meas} <0.7 than those authors reported. The ω_{meas} observed in near-source laboratory sampling as represented by the FLAME experiments does not capture the effects on the aerosol optical properties of water uptake or of aging processes that lead to deposition of secondary material. The addition of water and/or secondary species is expected to lead to increases in the visible-wavelength ω of the smoke aerosol. While the values of ω_{meas} reported here, particularly for the more highly absorbing samples, may not be applicable to ambient plumes or to aged smoke hazes, they are expected to represent an initial starting point for the aerosol optical properties. These initial conditions are useful for the validation of predictions of the evolution of smoke aerosol optical properties with age, and the resulting effects on direct aerosol forcing and visibility.

Acknowledgements. This research was supported by the US Department of Energy's Office of Science (BER) through the Western Regional Center of the National Institute for Climatic Change Research, Grant number MPC35TA-A4. The FLAME studies were supported by the US Joint Fire Science Program under JFSP Project Number 05-3-1-06, and by the National Park Service. The authors gratefully acknowledge the assistance of the many individuals who secured fuel samples for this work, and who helped conduct the burns described herein. We also thank the Joint Fire Science Program and the American Association for Aerosol Research for assisting with publication costs through their support of the Biomass Burning Symposium at the 2009 Annual Meeting of the AAAR.

References

Abo Riziq, A., Erlick, C., Dinar, E., and Rudich, Y.: Optical properties of absorbing and non-absorbing aerosols retrieved by cavity ring down (CRD) spectroscopy, Atmos. Chem. Phys., 7, 1523–1536, 2007, http://www.atmos-chem-phys.net/7/1523/2007/.

Anderson, T. L., Covert, D. S., Marshall, S. F., Laucks, M. L., Charlson, R. J., Waggoner, A. P., Ogren, J. A., Caldow, R., Holm, R. L., Quant, F. R., Sem, G. J., Wiedensohler, A., Ahlquist, N. A., and Bates, T. S.: Performance characteristics of a high-sensitivity, three-wavelength, total scatter/backscatter nephelometer, J. Atmos. Ocean. Technol., 13, 967–986, 1996.

Anderson, T. L. and Ogren, J. A.: Determining aerosol radiative properties using the TSI 3563 integrating nephelometer, Aerosol Sci. Technol., 29, 57–69, 1998.

Arnott, W. P., Moosmüller, H., Rogers, C. F., Jin, T. F., and Bruch, R.: Photoacoustic spectrometer for measuring light absorption by aerosol: instrument description, Atmos. Environ., 33, 2845–2852, 1999.

Arnott, W. P., Moosmüller, H., and Walker, J. W.: Nitrogen dioxide and kerosene-flame soot calibration of photoacoustic instruments for measurement of light absorption by aerosols, Review of Scientific Instruments, 71, 4545–4552, 2000.

Bae, M. S., Schauer, J. J., DeMinter, J. T., Turner, J. R., Smith, D., and Cary, R. A.: Validation of a semi-continuous instrument for elemental carbon and organic carbon using a thermal-optical method, Atmos. Environ., 38, 2885–2893, 2004.

Bond, T. C.: Can warming particles enter global climate discussions?, Environ. Res. Lett., 2, 045030, doi:10.1088/1748-9326/2/4/045030, 2007.

Bond, T. C. and Bergstrom, R. W.: Light absorption by carbonaceous particles: An investigative review, Aerosol Sci. Technol., 40, 27–67, 2006.

Chakrabarty, R. K., Moosmüller, H., Garro, M. A., Arnott, W. P., Walker, J., Susott, R. A., Babbitt, R. E., Wold, C. E., Lincoln, E. N., and Hao, W. M.: Emissions from the laboratory combustion of wildland fuels: Particle morphology and size, J. Geophys. Res. Atmos., 111, D7, doi:10.1029/2005JD006659, 2006.

Chen, Y. and Bond, T. C.: Light absorption by organic carbon from wood combustion, Atmos. Chem. Phys., 10, 1773–1787, 2010, http://www.atmos-chem-phys.net/10/1773/2010/.

Chow, J., Watson, J., Chen, L., Arnott, W., and Moosmüller, H.: Equivalence of elemental

carbon by thermal/optical reflectance and transmittance with different temperature protocols, Environ. Sci. Technol., 38, 4414–4422 2004.
Chow, J., Watson, J., Pritchett, L., Pierson, W., Frazier, C. and Purcell, R.: The DRI thermal optical reflectance carbon analysis system – description, evaluation and applications in United-States air-quality studies, Atmos. Environ., 27, 1185–1201, 1993.
Chow, J. C., Watson, J. G., Chen, L. W. A., Chang, M. C. O., Robinson, N. F., Trimble, D., and Kohl, S.: The IMPROVE-A temperature protocol for thermal/optical carbon analysis: maintaining consistency with a long-term database, J. Air Waste Managem. Assoc., 57, 1014–1023, 2007.
Chýlek, P. and Wong, J.: Effect of Absorbing Aerosol on Global Radiation Budget, Geophys. Res. Lett., 22, 929–931, 1995.
Dick, W. D., Saxena, P., and McMurry, P. H.: Estimation of water uptake by organic compounds in submicron aerosols measured during the Southeastern Aerosol and Visibility Study, J. Geophys. Res.-Atmos., 105, 1471–1479, 2000.
Dinar, E., Riziq, A. A., Spindler, C., Erlick, C., Kiss, G., and Rudich, Y.: The complex refractive index of atmospheric and model humic-like substances (HULIS) retrieved by a cavity ring down aerosol spectrometer (CRD-AS), Faraday Discussions, 137, 279–295, 2008.
Garland, R. M., Ravishankara, A. R., Lovejoy, E. R., Tolbert, M. A., and Baynard, T.: Parameterization for the relative humidity dependence of light extinction: Organic-ammonium sulfate aerosol, J. Geophys. Res., 112, D19303, doi:10.1029/2006JD008179., 2007.
Hand, J. L., Day, D. E., McMeeking, G. M., Levin, E. J. T., Carrico, C. M., Kreidenweis, S. M., Malm, W. C., Laskin, A., and Desyaterik, Y.: Measured and modeled humidification factors of fresh smoke particles from biomass burning: role of inorganic constituents, Atmos. Chem. Phys. Discuss., 10, 4225–4269, 2010, http://www.atmos-chem-phys-discuss.net/10/4225/2010/.
Hand, J. L. and Kreidenweis, S. M.: A new method for retrieving particle refractive index and effective density from aerosol size distribution data, Aerosol Sci. Technol., 36, 1012–1026, 2002.
Levin, E. J. T., McMeeking, G. R., Carrico, C., Mack, L., Kreidenweis, S. M., Wold, C. E., Moosmüller, H., Arnott, W. P., Hao, W. M., J. L. Collett, J., and Malm, W. C.: Biomass burning smoke aerosol properties measured during FLAME 2, J. Geophys. Res.-Atmos., in review, 2010.
Lewis, K., Arnott, W. P., Moosmüller, H., and Wold, C. E.: Strong spectral variation of biomass

smoke light absorption and single scattering albedo observed with a novel dual-wavelength photoacoustic instrument, J. Geophys. Res.-Atmos., 113, D16, doi:10.1029/2007JD009699, 2008.
Massoli, P., Bates, T. S., Quinn, P. K., Lack, D. A., Baynard, T., Lerner, B. M., Tucker, S. C., Brioude, J., Stohl, A., and Williams, E. J.: Aerosol optical and hygroscopic properties during TexAQS-GoMACCS 2006 and their impact on aerosol direct radiative forcing, J. Geophys. Res., 114, D00F07, doi:10.1029/2008JD011604, 2009.
McMeeking, G. R., Kreidenweis, S. M., Baker, S., Carrico, C. M., Chow, J. C., Collett, J. L., Hao, W. M., Holden, A. S., Kirchstetter, T. W., Malm, W. C., Moosmuller, H., Sullivan, A. P. and Wold, C. E.: Emissions of trace gases and aerosols during the open combustion of biomass in the laboratory, J. Geophys. Res.-Atmos., 114, D19, doi:10.1029/2009JD011836, 2009.
Moosmüller, H., Chakrabarty, R. K., and Arnott, W. P.: Aerosol light absorption and its measurement: A review, J. Quant. Spectros. Rad. Trans., 110, 844–878, 2009.
Park, K., Kittelson, D. B., and McMurry, P. H.: Structural properties of diesel exhaust particles measured by transmission electron microscopy (TEM): Relationships to particle mass and mobility, Aerosol Sci. Technol., 38, 881–889, 2004.
Ramanathan, V. and Feng, Y.: Air pollution, greenhouse gases and climate change: Global and regional perspectives, Atmos. Environ., 43, 37–50, 2009.
Ramanathan, V., Li, F., Ramana, M. V., et al.: Atmospheric Brown Clouds: Hemispherical and regional variations in long-range transport, absorption, and radiative forcing, J. Geophys. Res., 112, D22S21, doi:10.1029/2006J008124, 2007.
Reid, J. S., Eck, T. F., Christopher, S. A., Koppmann, R., Dubovik, O., Eleuterio, D. P., Holben, B. N., Reid, E. A., and Zhang, J.: A review of biomass burning emissions part III: intensive optical properties of biomass burning particles, Atmos. Chem. Phys., 5, 827–849, 2005, http://www.atmos-chem-phys.net/5/827/2005/.
Slowik, J. G., Stainken, K., Davidovits, P., Williams, L. R., Jayne, J. T., Kolb, C. E., Worsnop, D. R., Rudich, Y., DeCarlo, P. F., and Jimenez, J. L.: Particle morphology and density characterization by combined mobility and aerodynamic diameter measurements, Part 2: Application to combustion-generated soot aerosols as a function of fuel equivalence ratio, Aerosol Sci. Technol., 38, 1206–1222, 2004.
Sullivan, A. P., Holden, A. S., Patterson, L. A., McMeeking, G. R., Kreidenweis, S. M., Malm, W. C., Hao, W. M., Wold, C. E. and Collett, J. L.: A method for smoke marker measurements and its potential application for determining the contribution of biomass burning from wildfires and

prescribed fires to ambient $PM_{2.5}$ organic carbon, J. Geophys. Res.-Atmos., 113, D22302, doi:10.1029/2008JD010216, 2008.

Ward, D. E. and L. F. Radke: Emission measurements from vegetation fires: A comparative evaluation of methods and results, in: Fire in the Environment: The Ecological, Atmospheric, and Climatic Importance of Vegetation Fires, edited by: Crutzen P. J., and Goldammer, J.-G., 53–76, John Wiley, Chichester, UK, 1993.

Table 1. List of burns analyzed in this work. ID: Burn ID as catalogued in McMeeking et al. (2009). ω_{meas}: single-scattering albedo determined from nephelometer and photoacoustic spectrometer measurements.

ID	Fuel	ω_{meas}	Fuel Type
235	Longleaf pine needles and wire grass	0.934±0.006	trees and grass
236	Black needlerush	0.918±0.008	grass
237	Oak and hickory	0.852±0.012	trees
238	Douglas fir needles and branches, fresh	0.527±0.015	tree
239	Douglas fir needles and branches, dry	0.958±0.004	tree
240	Florida palmetto leaves	0.428±0.012	southeastern shrub
241	Mississippi palmetto leaves	0.615±0.016	southeastern shrub
242	Rice straw	0.890±0.010	Asian fuel
243	Alaskan duff	0.970±0.003	duff
245	Rhododendron leaves	0.809±0.014	southeastern shrub
246	Black spruce needles and branches	0.666±0.017	tree
247	Douglas fir needles and branches, fresh	0.975±0.003	tree
248	Alaskan duff	0.990±0.002	duff
249	Wiregrass	0.853±0.012	grass
250	Chamise	0.429±0.009	desert shrub
251	Black needlerush	0.900±0.009	grass
252	Sagebrush	0.701±0.016	desert shrub
253	Longleaf pine needles	0.951±0.005	tree
254	Gallberry	0.446±0.012	southeastern shrub
255	Sugarcane	0.696±0.016	Asian fuel
256	White spruce	0.910±0.008	tree

ACPD
10, 7469–7494, 2010

Table 2. Assumed densities and refractive indices used to calculate n_{comp} and k_{comp}.

Species	Density [g cm^{-3}]	Refractive index
KCl	1.99[a]	1.49[a]
K_2SO_4	2.66[a]	1.50[a]
KNO_3	2.11[a]	1.50[a]
NH_4Cl	1.53[a]	1.55[a]
NaCl	2.16[a]	1.54[a]
$(NH_4)_2SO_4$	1.76[b]	1.53[b]
Al_2O_3	3.97[a]	1.77[a]
CaO	3.30[a]	1.83[a]
Organic Carbon	1.40[c]	1.55[c]
Elemental Carbon[d]	1.7	1.75–0.63i
	2.1	1.95–0.79i

[a] Lide (2008); [b] Tang (1996); [c] Dick (2000); [d] Bond and Bergstrom (2006).

ACPD
10, 7469–7494, 2010

Table 3. Retrieved complex refractive indices (n and k) and ω_{meas} for selected burns, using lognormal distribution fits to the aligned volume size distributions after shifting by the appropriate shape factor. The fit lognormal distribution is indicated as monomodal (M) or bimodal (B), N is the number of samples for which the fit was minimized, and χ^2/N the merit function for that experiment. The eighth column indicates an estimate of the shape factor obtained by comparing total mass concentrations derived from gravimetric filter measurements with those calculated from the size distributions and estimated densities (see text). The final column indicates the shape factor applied to derive the complex refractive indices in columns 6 and 7, and also used in the construction of Fig. 3.

Fuel	Distribution type	Fit	N	χ^2/N	n	k	Ratio of calculated to gravimetric mass concentration	Shape factor applied in this work
Rice straw	DMPS-only	B	10	0.141	1.538±0.053	0.012±0.001	0.99	1.07
Rhododendron leaves	DMPS-only	B	10	0.222	1.564±0.053	0.030±0.003	1.0	1.07
Chamise	DMPS-only	B	8	6.32	1.605±0.071	0.217±0.063	1.5	1.55
Black needlerush	DMPS+OPC	B	5	0.582	1.579±0.090	0.019±0.002	0.79	1.0
Sagebrush	DMPS-only	M	18	0.018	1.665±0.071	0.086±0.009	1.0	1.23
Alaskan white spruce	DMPS-only	M	7	0.568	1.553±0.053	0.011±0.001	0.91	1.08

ACPD
10, 7469–7494, 2010

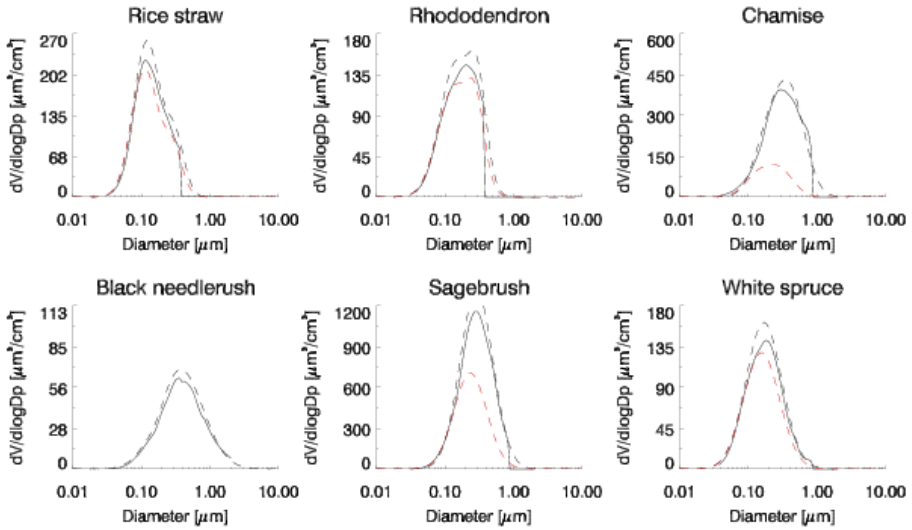

Fig. 1. Examples of measured aerosol size distributions (solid black lines) for six selected experiments. The dashed black lines indicate the lognormal fit size distributions. The dashed red lines indicate the lognormal fits for the size distributions after adjusting by the shape factors shown in Table 3.

ACPD
10, 7469–7494, 2010

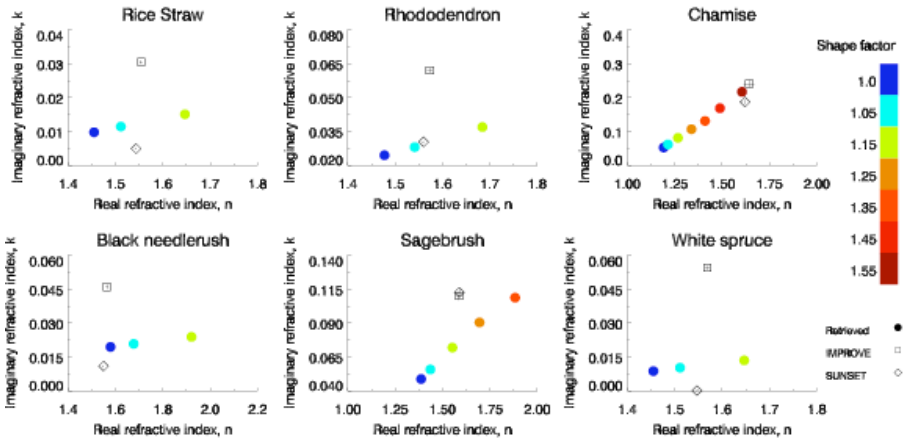

Fig. 2. Sensitivity of the retrieved real and imaginary components of refractive index (colored circles) to shifts in the measured size distribution (color bar indicates applied shape factor used to estimate effects of nonsphericity). The refractive index values computed from composition are shown as the black squares and diamonds, depending on the protocol used to obtain OC and EC concentrations.

ACPD
10, 7469–7494, 2010

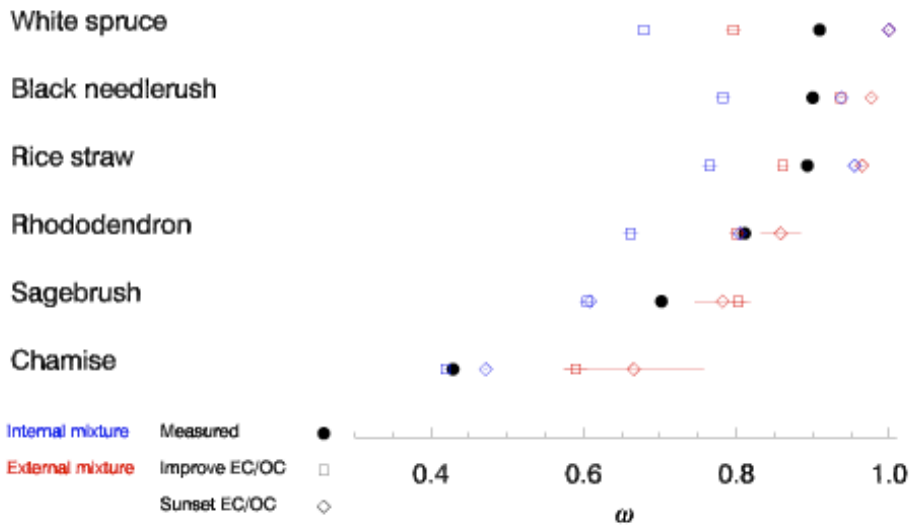

Fig. 3. Values of ω_{meas} derived from measured values of aerosol scattering and absorption coefficients (black circles). Blue and red symbols indicate ω calculated from aerosol composition using external (blue) and internal (red) mixture models, for two measurements of carbonaceous components: EC/OC values from the IMPROVE filters and TOR protocol (squares) and EC/OC values from the hi-vol filters analyzed by the Sunset instrument and NIOSH protocol (diamonds). Horizontal bars indicate the range of values produced by the extremes of EC properties (Table 2). In the composition-based calculations, the size distributions applied were those shifted by the shape factors indicated in Table 3.

ACPD
10, 7469–7494, 2010